PHYSICAL REVIEW B VOLUME 55, NUMBER 16 15 APRIL 1997-II

Structure and properties of cobalt clusters up to the tetramer: A density-functional study

Christine Jamorski
Département de Chimie, Université de Montréal, Case Postale 6128, Succursale Centre-Ville, Montréal, Québec, Canada H3C 3J7

Ana Martinez
Departamento de Química, División de Ciencias Básicas e Ingeniería, Universidad Autónoma Metropolitana-Iztapalapa, Apartado Postal 55-534, México, Distrito Federal 09340, Mexico

Miguel Castro
Departamento de Fisica y Química Teorica, Facultad de Química, Universidad Nacional Autonoma de México, Delegacíon Coyoacan, Ciudad Universitaria, Caixa Postale 04510, México, Distrito Federal, Mexico

Dennis R. Salahub
Département de Chimie, Université de Montréal, Case Postale 6128, Succursale Centre-Ville, Montréal, Québec, Canada H3C 3J7

(Received 25 November 1996)

All-electron calculations have been performed on cobalt clusters up to the tetramer using the local and generalized gradient correction spin density formalisms. These clusters present an abundance of low-lying states. In the case of Co_4, we have found that two and three-dimensional structures are energetically very close. Symmetric structures exhibit high degeneracy. Jahn-Teller deformations have hence been investigated and have been found to play an important role in such transition-metal clusters. General trends in the magnetic moment per atom and in the attachment energy have been elucidated. [S0163-1829(97)03616-3]

I. INTRODUCTION

Considerable effort is currently being expended on the study of transition-metal (TM) clusters, on the understanding that the knowledge gained can contribute to a better understanding of catalysis and be helpful in the development of new materials. At a more basic level, studying TM clusters allows us to characterize better metal-metal bonds and the associated electronic structure. Experimental data on cobalt clusters are sparse. They include estimates of the dissociation energy [1.69 eV (Ref. 1) and less than 1.32 eV (Ref. 2)] and of the vibrational frequency [290–296 cm^{-1} (Refs. 3 and 4) and 280 cm^{-1} (Ref. 5)] of the dimer, as well as studies of the variation of the ionization potential[2,6] (IP) and the magnetic moments[7–9] with the size of the cluster. Several experiments[7,10–15] have shown that the chemical and physical properties of clusters such as ionization potential, magnetic moment per atom, and attachment energies change with the size of the cluster, converging eventually to bulklike behavior.[16] The rate of convergence depends on the property that quantitative convergence often requiring tens, hundreds, or even more atoms. Clearly, only the most general qualitative aspects of the bulk materials would be reflected in the very small clusters ($n=1-4$) considered here. There appear to be no direct estimates available of the bond length and molecular parameters of cobalt clusters. There is also a scarcity of theoretical studies in the literature. The only cluster investigated until now is the dimer: Co_2 has been studied by extended Hückel,[17] restricted Hartree-Fock,[18] configuration-interaction,[19] and local spin density[20] methods.

For TM clusters, correlation effects are very important since they involve an open d shell giving rise to a number of low-lying states of high net spin number. We define the net spin number N_s as the difference between the number of α and β electrons for a given configuration and those spin configurations will be referred to hereafter as spin states. To find the more stable structures in a given range of energy, several structures and spin states have to be considered. The Jahn-Teller effect must also be taken into consideration since orbital degeneracy can occur in highly symmetric systems. The present work constitutes a theoretical study of cobalt clusters up to the tetramer with the local spin density approximation (LSDA) and the generalized gradient approximation (GGA) of density-functional theory (DFT). Related work on other metal clusters has already appeared.[21–23]

In the next section, we will discuss the details of the computations. Then, in Sec. II, we validate the method with respect to the quality of the grid and the choice of the auxiliary basis set necessary for DFT calculations on cobalt clusters. In Sec. III, our results will be presented and discussed.

II. COMPUTATIONAL DETAIL

The linear combination of Gaussian-type orbitals density-functional program DEMON-KS (Refs. 24 and 25) was used to perform all-electron calculations on cobalt clusters. In Demon-KS, the charge density and exchange-correlation (XC) potentials are expanded with auxiliary sets of Cartesian Gaussian functions and the final XC energy is evaluated by numerical integration on a grid (see Ref. 25 and references therein). The Vosko-Wilk-Nusair[26] parametrization was employed for LSDA calculations, while the GGA calculations were performed with the exchange gradient correction of Perdew and Wang[27] and the correlation gradient correction proposed by Perdew.[28,29] Unless otherwise specified, all calculations were performed with the grid option FINE of Demon-KS[30] which uses 832 points per atom for fitting the XC terms during self-consistent field (SCF) cycles and, once converged, 2968 points per atom to evaluate the final XC energy. This augmented grid is also used in the evaluation of the XC contribution to the gradient. The keyword NONRANDOM, meaning that the spherical shells of the grid were not randomly rotated, was specified to be consistent with the symmetry of some clusters. An orbital basis set of contraction pattern (63321/5211*/41+) (labeled DZVP, although no *f* functions are included) was used in conjunction with the corresponding (5,5;5,5) auxiliary basis set.[31] Several sizes of auxiliary basis sets were tested in dimer calculations to test the influence of the auxiliary basis set on calculated molecular parameters. Geometry optimizations were performed with a convergence criterion of 10^{-6} a.u. on the energy and 10^{-3} a.u. on the charge density. For the more stable structures, the optimized geometry and the vibrational analysis were computed with a more stringent convergence criterion (10^{-5} a.u.) on the charge density. Geometry optimizations were performed with the Broyden-Fletcher-Goldfarb-Shanno (BFGS) algorithm.[32]

Finally, unless otherwise stated, all calculations were performed with the SMEAR option. This option imposes fractional occupation number on the molecular orbitals in a given window range around the Fermi level. It does not exclude the possibility of having integral occupation number in cases where there is no degeneracy or pseudodegeneracy around the Fermi level. It is a well-known useful trick without which it would not have been possible to perform TM cluster calculations. It gave us the opportunity to compute highly symmetric structures for degenerate states. A detailed discussion of the side effects of this option will be given in Sec. IV. The LEVELSHIFT option has been used to aid convergence in those cases where the SMEAR option was not used. LEVELSHIFT increases the highest occupied molecular orbital (HOMO) to lowest unoccupied molecular orbital (LUMO) energy gap, thereby improving the convergence in quasi degenerate cases. Demon-KS uses a Carbo-like level shift operator.[33]

All-electron full geometry optimizations at the LSDA level were performed for all neutral clusters considered. Only the most stable LSDA structures were also computed at the GGA level. The two electronic configurations $4s^2\,3d^7$ and $4s^1\,3d^8$ of the atom were computed using the spherical (fractional occupation numbers) and nonspherical (NS) (integral occupation numbers) density approximation. Except for $Co_2{}^+$, cationic clusters were treated at both LSDA and GGA levels at the optimized ground-state geometry of their neutral counterparts. The range of spin states chosen varies according to the system studied. Specifically, the net spin numbers 2, 4, and 6 were studied for Co_2; 3, 5, and 7 for Co_3; and 4, 6, 8, 10, and 12 for the cobalt tetramer. In each case, we first optimized the geometry of the most symmetric structures in two and, where applicable, three dimensions. The cluster was then distorted so as to lower the symmetry and optimized again, and so forth until real frequencies and integral occupation numbers were found for the structures and spin states in this symmetry branch. A vibrational analysis was performed at both the LSDA and GGA levels on the most stable structures so as to discriminate between true minima and other types of stationary states.

The result of this procedure was a careful theoretical treatment of the following structures: the linear trimer, the equilateral triangle, and both acute and obtuse isosceles triangles of the trimer; the tetrahedron (T_d), both C_{3v} and D_{2d} structures obtained from a distortion of the tetrahedron, and the D_2 structure obtained from the distortion of the D_{2d} structure for the tetramer. Finally, the square and its two Jahn-Teller distorted geometries, the rectangle and the rhombus, as well as the C_{2v} structure obtained from the out-of-plane deformation of the rhombus, were also treated. Binding energies computed at the GGA level with the NS approximation should be regarded as our most reliable estimate.

TABLE I. Molecular parameters of Co_2 and Co_2^+ evaluated by severals methods. Values in parentheses were calculated with an extra-fine grid.

Calculation type	LSDA		GGA	
	R_e (Å)	ω_e (cm^{-1})	R_e (Å)	ω_e (cm^{-1})
	Co_2 neutral			
BFGS (5,5;5,5)	1.92	444	1.95	421
BFGS (4,4;4,4)[a]	1.92	445	1.95	420
BFGS (6,6;6,6)[a]	1.92	439	1.95	414
BFGS (8,8;8,8)[a]	1.92	441	1.95	418
fit E_{fit}[b]	1.91 (1.92)	476 (449)	1.94 (1.95)	502 (550)
fit E_{num}[c]	1.93 (1.93)	385 (400)	2.01 (2.01)	342 (353)
$E^{(1)}_{\mathrm{user\ grid}}$[d]			1.99	355
$E^{(2)}_{\mathrm{user\ grid}}$[e]			1.99	357
	$Co_2{}^+$			
BFGS (5,5;5,5)	1.94	415	1.96	432
fit E_{fit}[a]	1.93	466	1.97	457
fit E_{num}[b]	1.95	366	2.02	377

[a] Generated with the general recipe given in Ref. 31.

[b] From the second-order polynomial fit of the energy calculated using fitting.

[c] From the second-order polynomial fit of the energy calculated by numerical integration.

[d] In this row; the optimized geometry was calculated with a user grid of 128 and 194 radial and angular points, respectively. The frequency was calculated using a simple parabolic fit of the single-point calculation calculated with the user grid.

[e] In this row, the optimized geometry was calculated with a user grid of 200 and 194 radial and angular points, respectively. The frequency was calculated using a single parabolic fit of the single-point calculation calculated with the user grid.

III. VALIDITY OF THE METHOD

Co_2 has been used to test the quality of our results compared to our best estimate of the limit of the method in the context of a chosen functional. Once the functional has been chosen, we still have to test the quality of the orbital and auxiliary basis set as well as the size of the grid. Many orbital basis sets were used in conjunction with a (5,5;5,5) sized auxiliary set (built in the spirit of Ref. 31) to compute the cobalt atom and dimer. The only basis set that gives reasonably good results is the one kept in this work. In Table I we have reported the bond length and the frequency computed with a parabolic fit of the numerical energy (details are given later). We did this to eliminate three sources of error,

TABLE II. Total energy (a.u.) of the $4s^23d^7$ and $4s^13d^8$ configurations calculated at the LSDA and GGA levels with the spherical and NS approximations.

Electronic configuration	Spherical		Nonspherical	
	LSDA	GGA	LSDA	GGA
$4s^23d^7$	−1379.876 080	−1382.752 161	−1379.908 459	−1382.803 386
$4s^13d^8$	−1379.908 462	−1382.773 935	−1379.937 920	−1382.802 226
ΔE (eV)[a]	+0.881	+0.592	+0.802	−0.032

[a] $\Delta E = E(4s^23d^7) - E(4s^13d^8)$. The experimental separation is equal to 0.418 eV (Ref. 47).

that due to the size of the grid in the evaluation of the gradient, that due to the incompleteness of the exchange-correlation auxiliary basis, and that involved in the numerical calculation of the force constants by finite differences of the gradients. We can examine more directly the effect of grid size and auxiliary basis sets in the SCF and energy calculations as the limit for a particular functional is approached. Here we show that geometry optimization of the dimer places heavy demands on the grid. The quality and completeness of the auxiliary basis set is also very important. Incomplete basis sets could lead to significant changes in the calculated spectroscopic parameters (as seen in Ref. 34). In Table I we report results at both LSDA and GGA levels for the equilibrium bond length and frequency of Co_2 calculated with different sizes of auxiliary basis set [(4,4;4,4), (5,5;5,5), (6,6;6,6), and (8,8;8,8)]. The auxiliary basis sets were generated as in Ref. 31. Results computed with the (5,5;5,5) auxiliary basis set were chosen for use in all our calculations. Those results are labeled BFGS to emphasize the fact that they were computed with the BFGS optimization algorithm. Clearly, these results show that the auxiliary basis set chosen is reasonably complete.

Demon-KS computes two different energies, namely, the fitted energy and the numerical energy. The difference between those two numbers is in the way the XC energy is computed. In the fitted result, the XC energy density is fitted with the XC auxiliary basis set on a reduced set of grid points (832 points per atom for a FINE grid) and the XC energy is evaluated with this fitted quantity, while for the so-called numerical result, the XC energy is computed, at the SCF convergence, by direct numerical integration over an extended set of grid points (2968 grid points per atom for a FINE grid). To check the validity of the bond length and frequency calculated from the energy gradients, a series of points (seven in general) close to the minimum has been fitted using a simple parabolic fit. In Table I we have reported the bond length and frequency of Co_2 and Co_2^+ computed with either the BFGS algorithm [BFGS (5,5;5,5)], a parabolic fit of the fitted energy (fit E_{fit}), or a parabolic fit of the numerical energy (fit E_{num}). At the GGA level, we can see an important discrepancy between the BFGS and the fit E_{num} bond length and frequency for both dimers. An EXTRA FINE calculation of the fitted energies (Table I, results in parentheses) confirms this tendency. We use two USER defined grids to perform the optimization of the geometry: one with 128 radial points and 194 angular points giving 24 832 points per atom, and one with 200 and 194 radial and angular points, respectively, for a total of 38 800 points per atom. At the GGA level, both grids give an optimized bond length of 1.99 Å (see Table I, $E_{\text{user grid}}$), which is in agreement with the minimum of the fit of the numerical calculation. Hence, for the GGA calculations, the use of default grid options may lead to errors of several hundredths of an angstrom for metal-metal bond lengths. While this is acceptable for many purposes, it is clear that precise work will require extended grids. A minimally adequate grid for GGA calculations on transition-metal clusters has not yet been established, though there are indications that about 50 or 60 radial points will be required.[35,36] Similar conclusions about the need for attention to the grid have been reached by Baker *et al.*[37]

We have thus shown that geometry optimization of TM clusters places heavy demands on the grid. The largest grid used for the dimer is too demanding to use in treating clusters containing several atoms. Thus all others clusters calculations reported here were done with a FINE grid as described earlier in Sec. II. Though the precise values of the molecular parameters and energies could be affected (bond lengths by a few hundredths of an angstrom, frequencies by some tens of cm^{-1}, and close-lying isomers could be interchanged), we expect that the general trends should be valid.

IV. RESULTS AND DISCUSSION

A. Cobalt atom

The experimental ground state of the cobalt atom has the configuration $4s^23d^7$ and is a ^4F state. The first excited state has the configuration $4s^13d^8$ and is also a ^4F state. As in Hartree-Fock theory, the treatment of open-shell atoms in density-functional (DF) theory[38–42] is complicated by the multiplet problem. Formally, DF calculations on a given system should give the ground-state energy and charge density of the lowest state of this system. However, present XC functionals do not have the proper spatial and spin symmetry behavior to describe multiplet systems correctly. One way out of this dilemma is to use a linear combination of determinants instead of a single determinant. This is the spirit of the approach proposed by Messmer and Salahub[43] and by Ziegler, Rauk, and Baerends[44] and elaborated upon, more recently, by Daul[45] (see also Ref. 46 for a different approach to the multiplet problem[46]). In the present work, the atom is treated at the Kohn-Sham DF theory level without multiplet corrections. The energy so calculated may be thought of as averaged over the allowed states of the given multiplicity. In our case, it is a mixture of the ^4F and ^4P states for both ($4s^23d^7$ and $4s^13d^8$) configurations. It is important to note that, while the calculated value of the binding energy will be affected, this does not affect the relative stability of the different clusters, which is the main interest of this work.

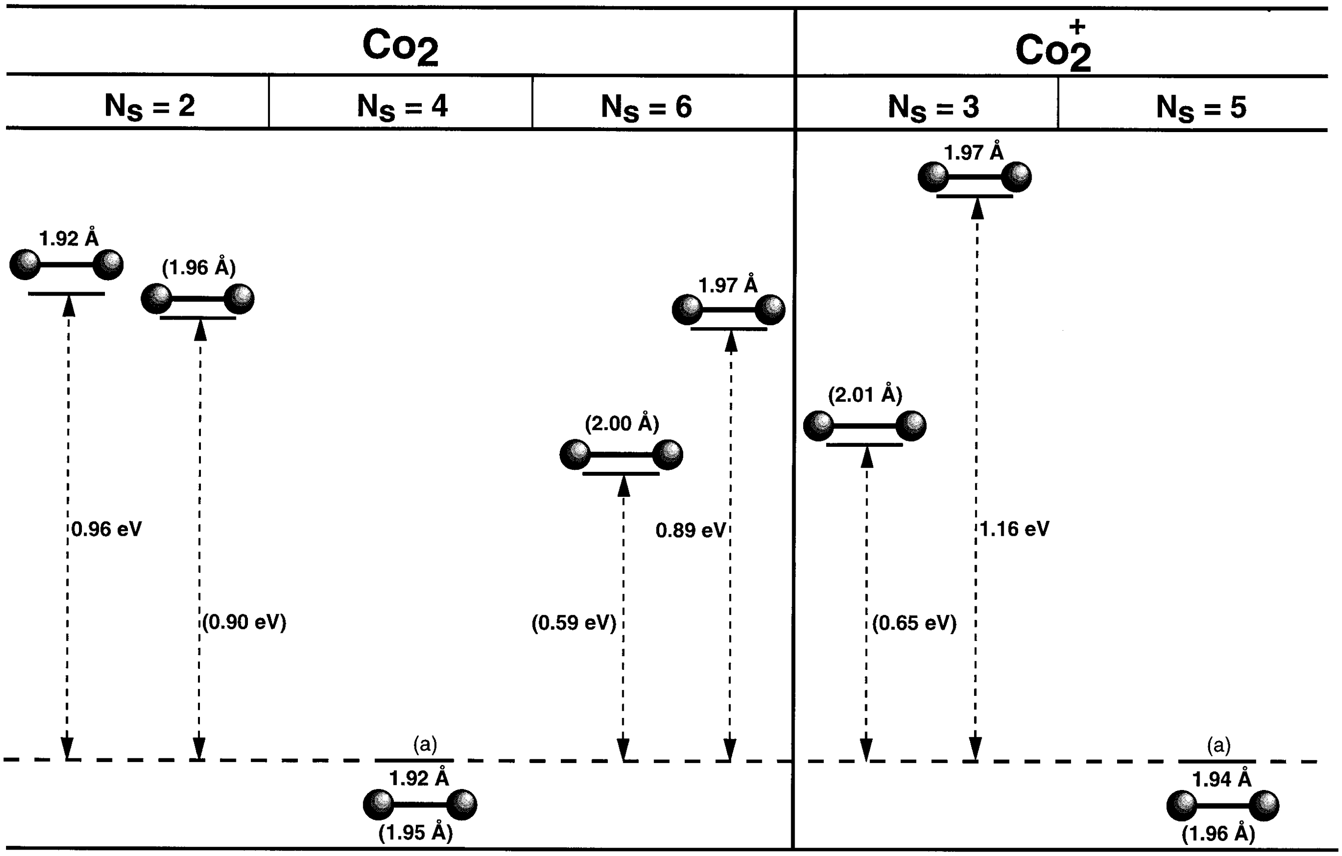

FIG. 1. Relative stability of LSDA and GGA Co_2 and ${Co_2}^+$ optimized structures. (a) Both LSDA and GGA ground states are artificially put at the same level for clarity.

Kutzler and Painter[42] have shown that at the GGA level, allowing the atomic density to be nonspherical improves the total energy of the atom and thus the binding energies of the molecular system under consideration. In Table II total energies are reported for both spherical and nonspherical atoms.

Usually, in DF calculations, the $4s^1 3d^{n-1}$ configuration is more stable than $4s^2 3d^{n-2}$. This was pointed out by Jones and co-workers.[40,41] We observe the same trend for both spherical and nonspherical atoms at the LSDA level; see Table II. This is also true for GGA calculations with spherical atoms. But for nonspherical atoms at the GGA level, the $4s^2 3d^7$ configuration is more stable, giving an interconfigurational separation of 0.032 eV compared with the experimental separation of 0.418 eV (Ref. 47) (averaged over the J states). Mlynarski and Salahub[48] have already observed this behavior for the nickel atom using the same gradient-corrected functional as in the present work. An extensive GGA study of the transition-metal atoms without the assumption of spherical symmetry would clearly be of interest.

B. Dimer

The most recent experimental data[2] predict that the binding energy of Co_2 is less than 1.32 eV,[2] which makes it difficult to study spectroscopically.[49] This could explain why there are practically no experimental (or theoretical) studies of the dimer in the literature.[1,4,5,50]

Our LSDA and GGA optimized structures of the neutral dimer and ion dimer are presented in Fig. 1 along with their relative stabilities. The ground state of the neutral dimer is found to be a $\Delta_g(N_s=4)$ state. The $\Delta_g(N_s=2)$ and $\Sigma_g(N_s=6)$ states are less than 1 eV above the ground state. The ground state of the cation is a $\Sigma_g(N_s=5)$ state, in agreement with electron spin resonance spectroscopy.[50] The $\Delta_g(N_s=3)$ excited state is around 0.65 eV higher, while the $\Sigma_g(N_s=7)$ state (which is not included in Fig. 1) is more than 2 eV higher.

The differences and similarities between the bond lengths of the different states of each dimer can be explained on the basis of the molecular orbitals (MO's) whose energy and fillings are shown in Figs. 2 and 3 for Co_2 and Co_2^+, respectively. For the neutral dimer, from Fig. 2, we can see that to go from the $N_s=4$ to 2, one must free a $\delta_u^{*\alpha}$ antibonding MO to occupy a $\delta_u^{*\beta}$ antibonding MO. The nature of the bond does not change and consequently the bond length of those two states are equal at the LSDA level (and almost equal at the GGA level). On the other hand, to go from the ground state ($N_s=4$) to $N_s=6$ one must free an antibonding $\delta_u^{*\beta}$ MO to occupy a more antibonding $4s(\sigma_u^{*\alpha})$ MO. In so doing, the relative order of the valence MO's changes. In this case the nature of the bond is perturbed and we observe an elongation due to the $4s(\sigma_u^{*\alpha})$ antibonding MO. Finally, the small experimental binding energy of less than 1.32 eV ob-

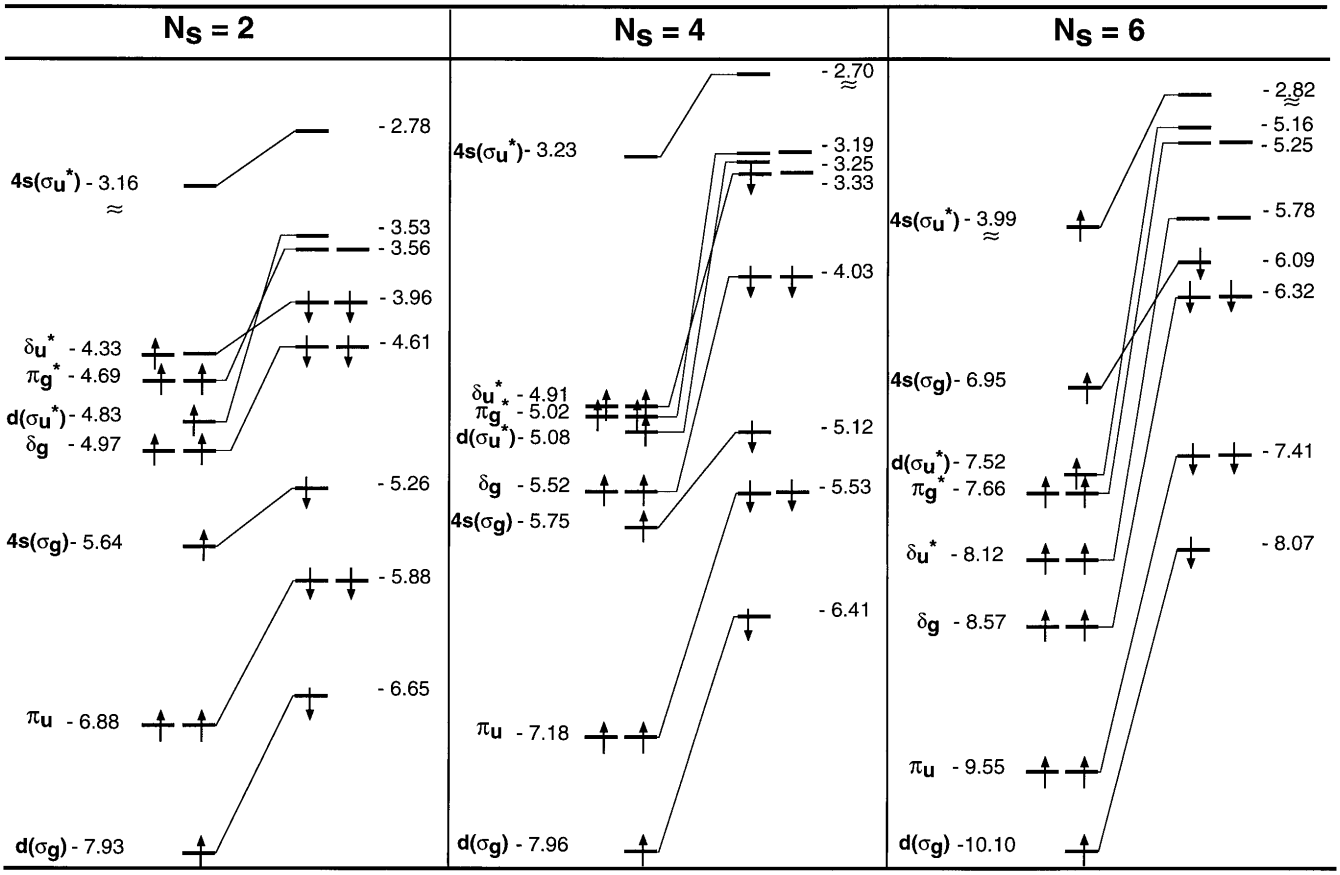

FIG. 2. Molecular diagram of the dimer $\Delta_g(N_s=2)$, $\Delta_g(N_s=4)$, and $\Sigma_g(N_s=6)$ states.

served for Co$_2$ (Ref. 2) may be rationalized by the contribution of antibonding MO to the bond.

The same sort of discussion holds for the cationic dimer (see Fig. 3), except that in this case we observe an elongation of the bond for both excited states. Namely, to go from $N_s=5$ to 3, one must free a $4s(\sigma_g^\alpha)$ bonding orbital to occupy a $\delta_u^{*\beta}$ antibonding orbital, consistent with the observed small elongation of the bond length. The $N_s=7$ spin state is obtained if one transfers an electron from the $4s(\sigma_g^\beta)$ bonding MO of the $N_s=5$ spin state to occupy a $4s(\sigma_u^{*\alpha})$ antibonding orbital, leading to an important elongation (2.09 Å) of the bond length.

In Table III we have reported the equilibrium bond length, frequency, binding energy, and IP of Co$_2$ computed with the fit of the numerical energy (see Sec. IV C for more details) along with experimental and other theoretical results. There is no experimental bond length, except for the estimated bond length of Kant and Strauss,[1] 2.31 Å, calculated from the Pauling radius. Our bond length is shorter than other calculated equilibrium distances, but we have confidence in this value (2.01 Å at the GGA level) since the experimental bond length of the neighboring dimers Fe$_2$ and Ni$_2$ are 1.87 Å (Ref. 51) and 2.02 Å (Ref. 52) [or 2.155 Å (Ref. 53)], respectively. It is interesting to note that Harris and Jones LSDA calculation,[40] as well as our calculation, predict a $^5\Delta_g$ ground state with a bond length around 2 Å, while the configuration-interaction (CI) calculation of Shim and Gingerich[19] predicts a $^5\Sigma_g$ ground state with a longer distance. This last calculation is not extensive since it was limited to only 1084 configurations. Nevertheless, due to its electronic structure, Co$_2$, as well as Fe$_2$ and Ni$_2$, has many low-lying states, and this $\Sigma_g(N_s=4)$ state could be one of them. To clarify this situation, we attempted to compute the potential surface, but were prevented from completing this project by convergence problems. But, indeed, around 2.37 Å, we did observe an inversion in the stability of the occupied $\delta_u^{*\beta}$ orbital and the unoccupied $\sigma_u^{*\beta}$ orbital, which leads to a $\Sigma_g(N_s=4)$ state. Recently, doing CI calculations on Fe$_2$, Tomonari and Tatewaki[54] have found two local minima, corresponding, respectively, to $\Delta_u(N_s=6)$ and $\Sigma_u^+(N_s=6)$ states at 2.02 and 2.60 Å. We may thus expect to find such weakly bound Σ states for the cobalt dimer too.

In Co$_2$, each atom has approximately a $4s^1 3d^8$ configuration. Shim and Gingerich[19] found that the $3d$ orbitals do not participate in the bond, in contradiction with our results where Mayer bond order analysis indicates a triple bond. Our GGA computed frequency is in agreement with that of Harris and Jones and in the range of the experimental results. The observed discrepancy of about 50 cm^{-1} is common in Demon-KS calculations for TM's and represents a combination of numerical errors, intrinsic errors of the functional and anharmonicity. The binding energy and IP were computed at the bond length of the fit of the numerical energy. The binding energy was computed at the GGA level using the nonspherical reference atom also treated at the GGA level. Nevertheless, satisfactory agreement with the experimental results is not attained. This is clearly related to the poor description of the atom, which is a well-known problem in

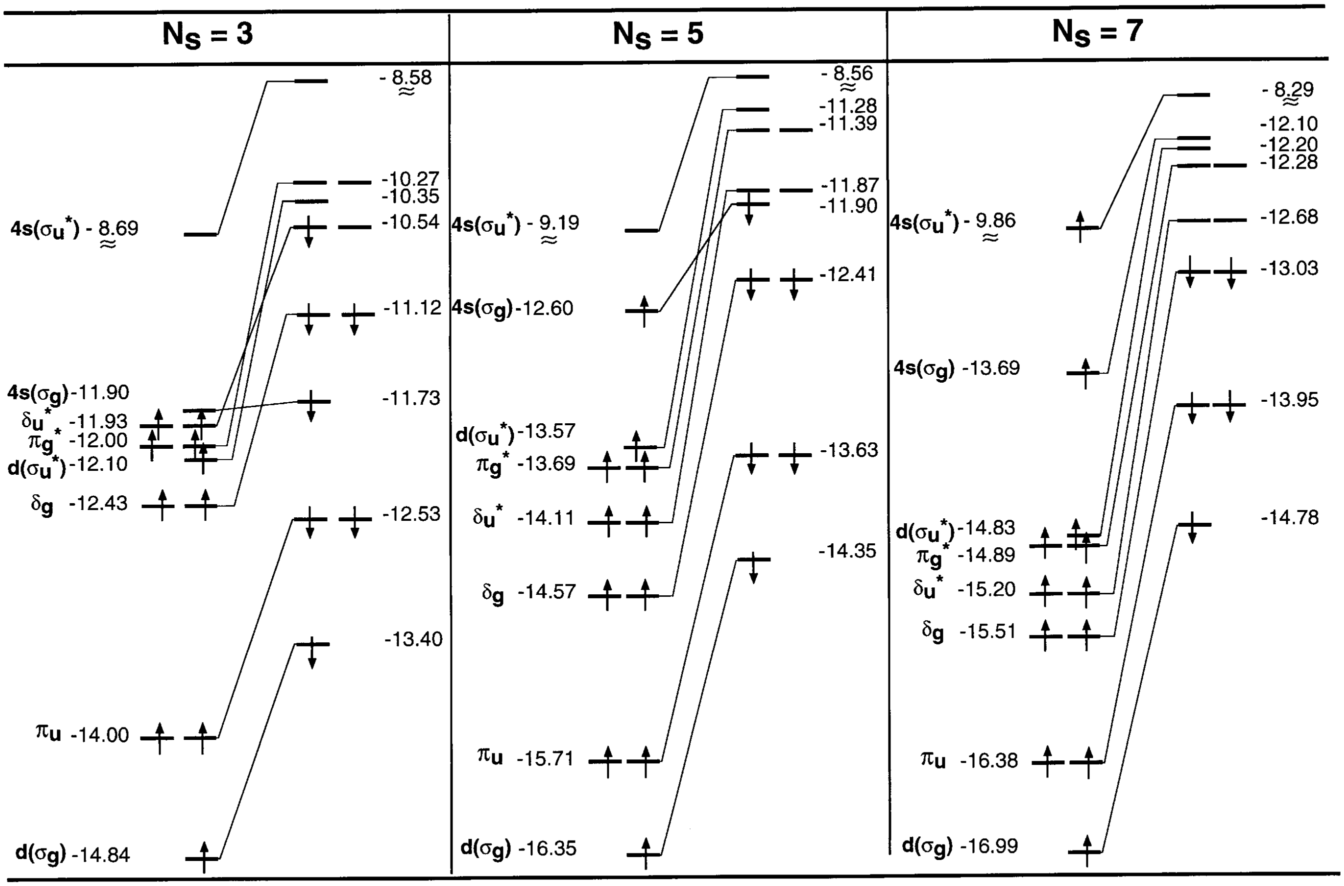

FIG. 3. Molecular diagram of the $\mathrm{Co}_2{}^{+}$ $\Delta_g(N_s\!=\!3)$, $\Sigma_g(N_s\!=\!5)$, and $\Sigma_g(N_s\!=\!7)$ states.

DFT. But we will see later that, despite this, the experimental trends are reproduced for the set of clusters studied here. Our calculations overestimate the experimental IP by 1.2 eV, but this value is still in better agreement with experiment than IP's calculated using others methods. Only a small improvement is observed with the GGA functional.

C. Trimer

The trimer structures optimized at the LSDA level are presented in Fig. 4, with $N_s\!=\!3$, 5, and 7. Our calculations show that the equilateral triangles are more stable than the linear structures for all spin states considered. Given the energy difference between linear and planar structures, their

TABLE III. Comparison of Co_2 R_e (Å), ϵ_e (cm^{-1}), D_e (eV), and IP (eV) calculated at LSDA and GGA levels with other theoretical calculations and experimental results.

	State	R_e (Å)	ω_e (cm^{-1})	D_e (eV)	IP (eV)	Ref.
LSDA	$^5\Delta_g$	1.93	385		7.58	
GGA	$^5\Delta_g$	2.01	342	2.26	7.48	
extended-Hückel		2.30	370	1.63	9.2	17
(two parametrization)		2.30	410	1.84	11.5	17
LSD	$^5\Delta_g$	2.07	360	3.35		40
CI	$^5\Sigma_g$	(2.56)[a]	162	0.81		19
experimental		(2.31)[b]	290			3
			280±20			5
					6.26±0.16	6
				≤1.32	6.42	2
				0.7–1.4		50
			296.8±5.4			4

[a] A value from a limited CI calculation, likely to be seriously too long (see the text).

[b] An early estimate based on Pauling radii and general trends observed in organic molecules.

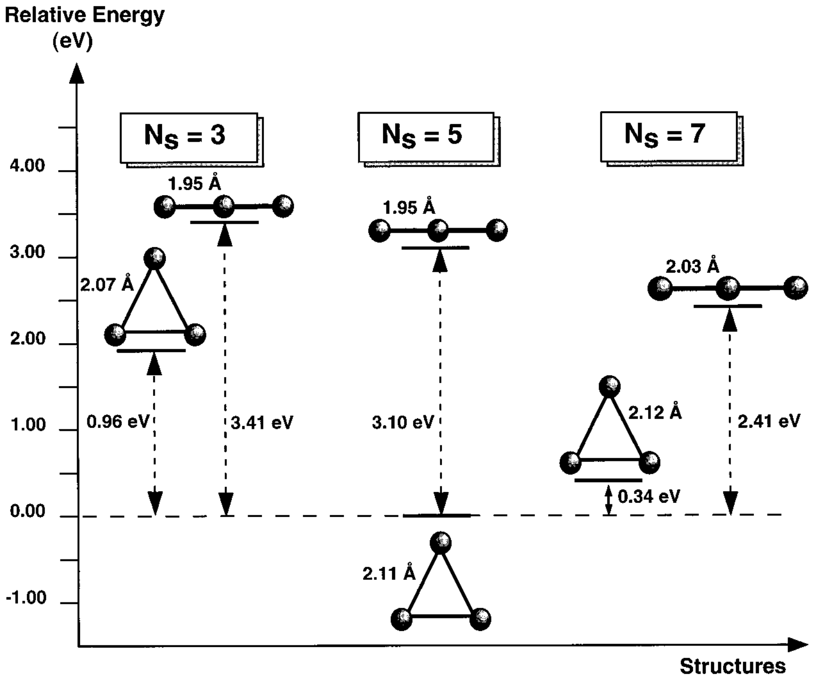

FIG. 4. Relative stability of the linear and D_{3h} LSDA optimized structures of Co_3.

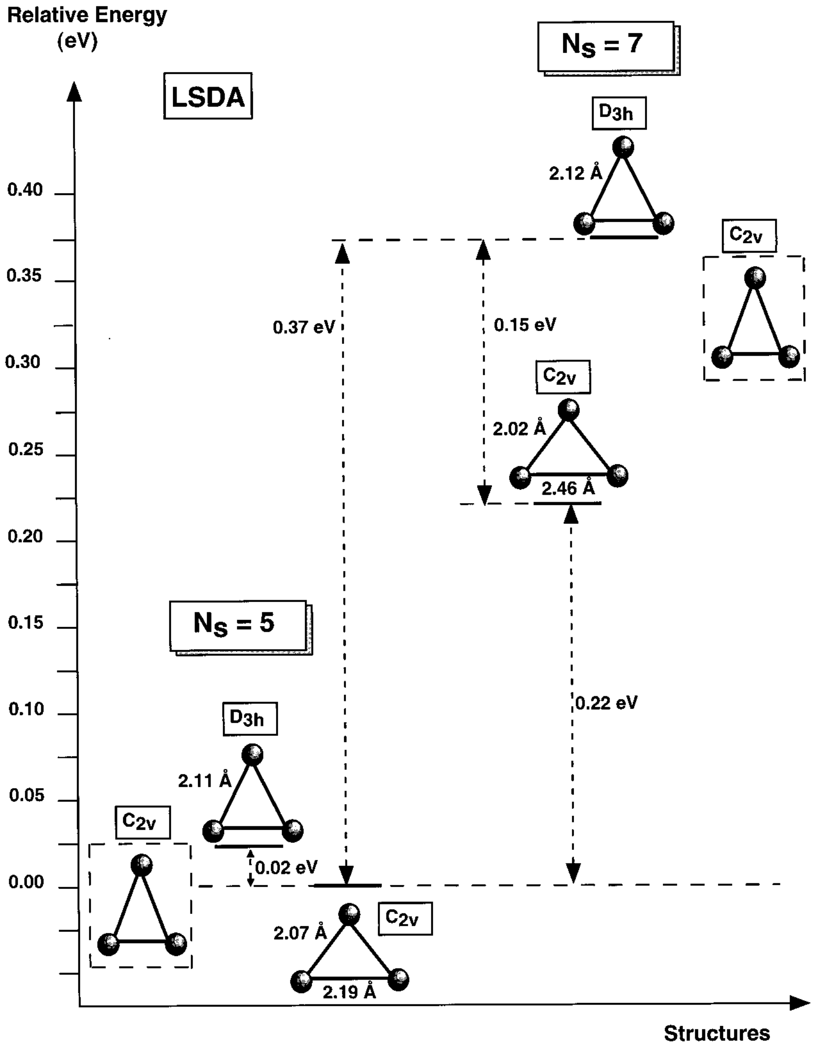

FIG. 5. Relative stability of the Jahn-Teller distorted structure for Co_3.

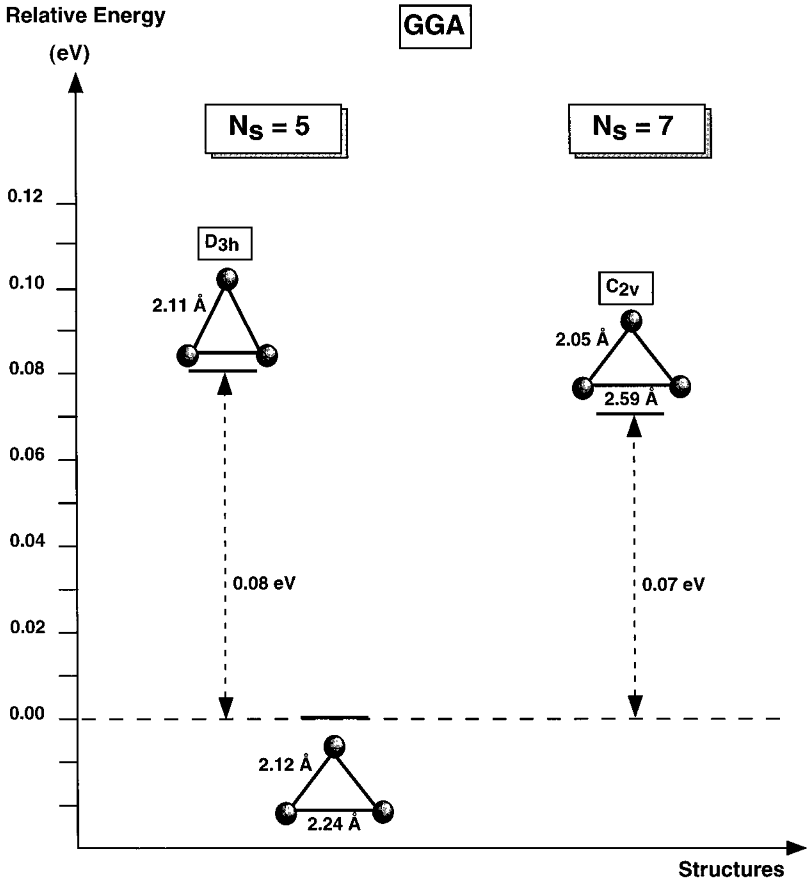

FIG. 6. Relative stability of the Co_3 GGA optimized structures.

relative stability should be the same at the GGA level. The same assumption is made for the triangle of with $N_s = 3$ since it is roughly 1 eV less stable than the other two triangles. We can thus focus our attention on the equilateral triangles with $N_s = 5$ and 7 and their Jahn-Teller distorted structures. Considering the occupation of the MO's and their degeneracy, we can see that the HOMO's of both structures are doubly degenerate and half occupied. Thus these structures have states of E symmetry. Therefore, they are subject to a first-order Jahn-Teller (FOJT) deformation along the E' vibrational mode. This could lead to two possible structures of C_{2v} symmetry, namely, the acute and obtuse isosceles triangles.

Figure 5 shows the relative stability of the isosceles triangleswith $N_s = 5$ and 7 computed at the LSDA level. The acute triangles are shown as dashed squares since it was not possible to obtain those structures using the standard optimization procedure. A more detailed description of the problem will be given at the end of this section. The most stable structure at this level is the obtuse triangle with $N_s = 5$ that is 0.02 eV lower than the $D_{3h}(N_s = 5)$ structure. As a general trend, we can see that the bond length of the equilateral triangles does not change (within the 0.05-Å accuracy range of the calculation) with the net spin number, while for the isosceles triangles, the longest bond length increases with the net spin number.

GGA structures are presented in Fig. 6. The equilateral triangle with $N_s = 7$ does not appear to be a minimum. Optimization led to the obtuse triangle. The general tendencies observed for LSDA geometries still apply at the GGA level as well as the note concerning the problem with acute triangles. The $D_{3h}(N_s = 5)$ and $C_{2v}(N_s = 7)$ structures are less

TABLE IV. Spectroscopic constants of the Co_3 $N_s = 5$ obtuse triangle.

				Vibrational frequencies		
	R_e (Å)	D_e (eV)	Vertical IP (eV)	Assignment	Spectral activity	ν (cm^{-1})
LSDA	$r_1 = 2.187$	8.36[a]	6.59	a_1	IR	233
	$r_2 = 2.074$			b_2	IR,R	260
				a_1	IR	400
GGA	$r_1 = 2.242$	4.60	6.60	a_1	IR	220
	$r_2 = 2.117$			b_2	IR,R	235
				a_1	IR	372

[a] D_e performed with the atom calculated at the LSDA level using the NS approximation, see Table II.

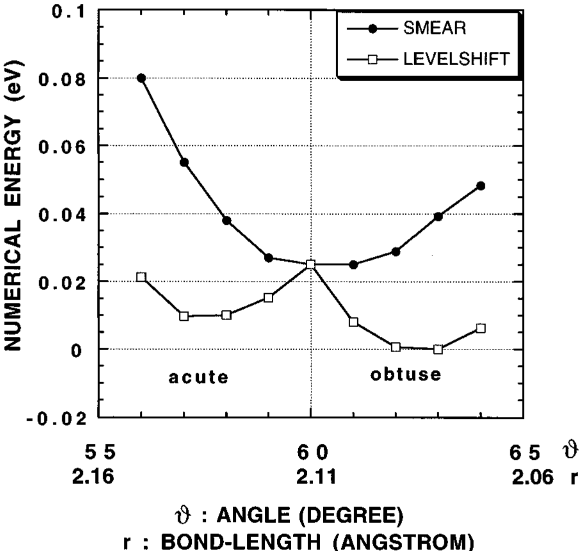

FIG. 7. Cut of the Co_3 symmetry restricted (isosceles triangle) LSDA adiabatic potential surface. The variable r represents the bond length of identical sides of the isosceles triangle, while Θ is the angle between those two sides.

stable than the $C_{2v}(N_s=5)$ by 0.08 and 0.07 eV, respectively. Those three structures are contained in a range of 0.1 eV and thus an assignment of the ground state to one particular structure is not appropriate. Frequencies, dissociation energy, and vertical IP were computed only for the $C_{2v}(N_s=5)$ structure; see Table IV. The frequencies show that this structure is a real minimum on the adiabatic potential surface.

We now return to the acute triangle problem mentioned earlier. Figure 7 represents LSDA single-point calculations computed at different r and Θ values with the SMEAR and LEVELSHIFT option, where r is the bond length of the identical sides of the isosceles triangle, while Θ is the angle between those two sides. A different behavior is observed according to the option chosen: LEVELSHIFT or SMEAR. With the SMEAR option, the adiabatic potential surface (APS) has a minimum for the $D_{3h}(N_s=5)$ structure, while with the LEVELSHIFT option both acute and obtuse triangles are minima and the $D_{3h}(N_s=5)$ structure is at the cusp point of the APS. In order to have a clear picture of the APS in the region of the three triangles, single-point calculations were performed at the LSDA level. Results are presented in Fig. 8 as a contour map of the APS. The diagonal line in this figure corresponds to the section of the APS shown in Fig. 7, while the crosses the Demon-KS optimized obtuse triangle. This cross is clearly not situated at the guessed minimum of the obtuse triangle part of the APS. This discrepancy reflects the same tendency observed for Co_2, where the parabolic fit of the numerical energy yields a somewhat different bond length from the one computed by the gradient optimization and is probably related to the quality of the grid used. It can be seen from Fig. 7 that the energetic barrier between the acute and obtuse triangle is only 0.02 eV and thus only the first vibronic level of the obtuse triangle is contained in the well. The energy difference between the two triangles is 0.005 eV, thus we cannot give more importance to one of these structures.

D. Tetramer

The study of the tetramer is clearly more complex than that of the trimer since more structures and spin states are involved. Jahn-Teller effects[55] prevent these clusters from adapting their most compact and symmetrical forms. The vibrational modes involved in the first- and second-order Jahn-Teller (JT) deformations for the structures investigated are shown on Fig. 9. With JT effects in mind, we start our investigation of CO_4 with the most symmetrical two-dimensional (D_{4h} symmetry) and three-dimensional (T_d symmetry) structures, from which should be obtained less symmetrical structures of higher stability. Spectroscopic constants will be presented for the most stable structure $D_{2d}(N_s=10)$. The section ends with a discussion of the ac-

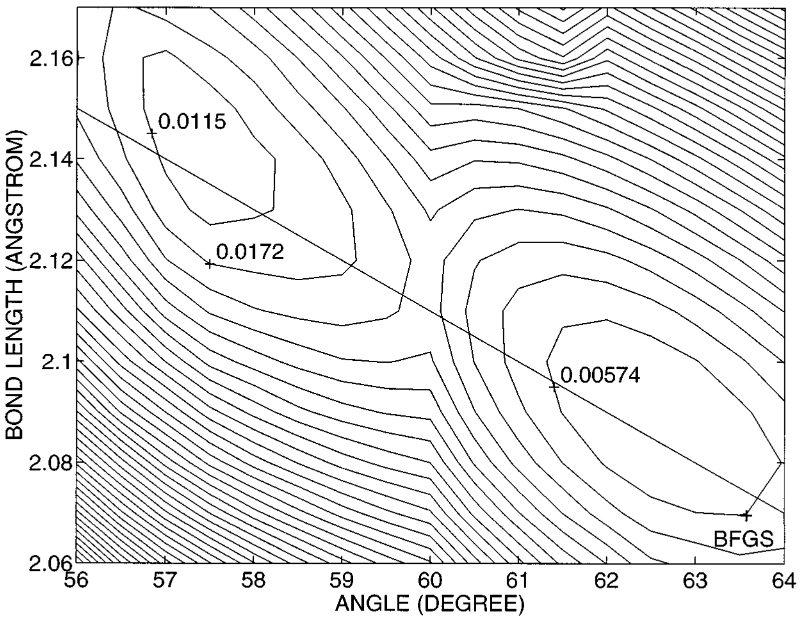

FIG. 8. Contour map of Co_3 symmetry restricted (isosceles triangle) LSDA adiabatic potential surface.

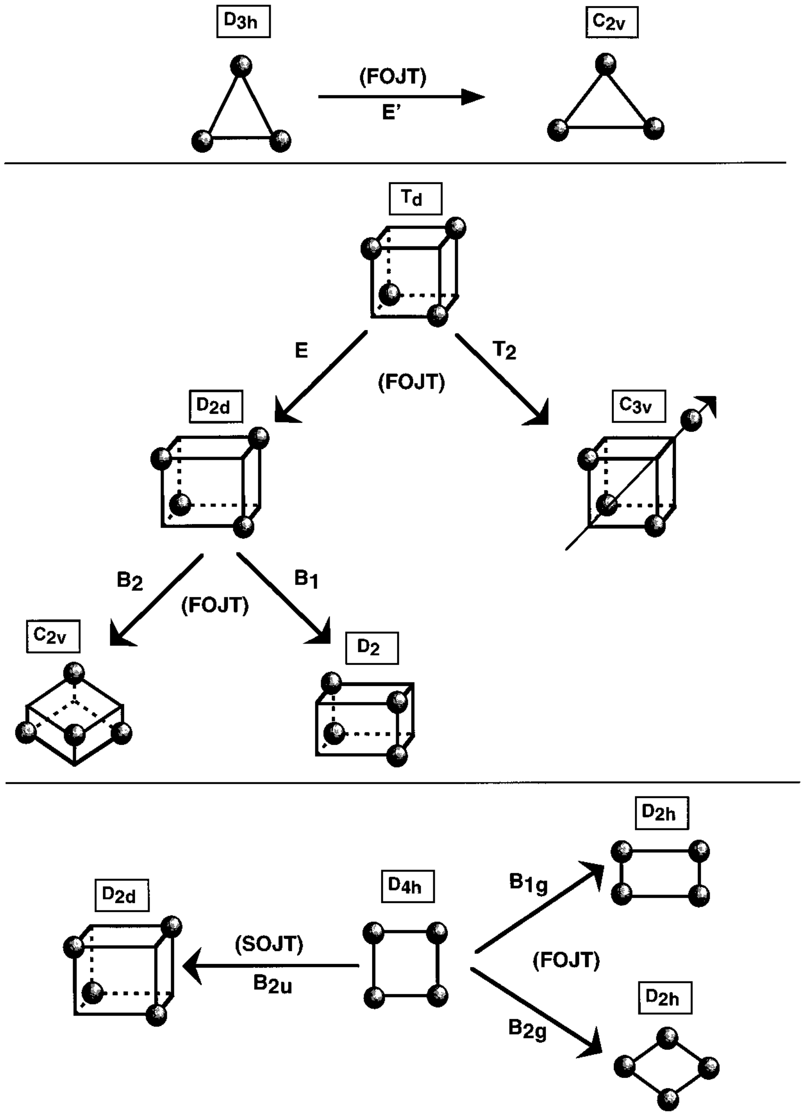

FIG. 9. First- and second-order JT distorted structures of several structures.

curacy of the calculations, and a general conclusion about the level of calculation necessary for transition metal clusters will be given.

1. Analysis of the results

In order to systematize the investigation of the potential surface, the most symmetrical structures D_{4h} and T_d were considered, as a first approximation, for several multiplicities. When appropriate, the symmetry of those structures was reduced according to the active JT modes or according to the mode of vibration involving an imaginary frequency. The vibrational analysis takes an important place here since it can give us information about the nature of the state. The strategy adopted is to consider GGA vibrational calculations more reliable than LSDA ones (see Sec. III). The numerical error (about 50 cm^{-1}) of the vibrational calculation will also be taken into account. All structures computed at the LSDA level are summarized in Table V. GGA results are presented in Tables VI and VII.

(a) Highly symmetrical structures: D_{4h} and T_d. The optimized T_d and D_{4h} structures calculated at the LSDA level for $N_s=6$, 8, and 10, are presented in Fig. 10. As a general trend, the T_d structure bond length is longer than the D_{4h} one. Note that if we had restricted ourselves to compute only the highest symmetrical structures, the most stable one would have been the square with $N_s=10$. But, as we will see shortly, JT distorsions play an important role here. A closer inspection of the MO's of all the square conformers shows that the HOMO's are doubly degenerate and half occupied. Those structures are thus subject to a FOJT deformation along the B_{1g} and B_{2g} vibrational modes. Furthermore, the vibrational analysis ($N_s=8{,}10$ only) shows imaginary frequencies for the same vibrational modes, which means that both deformations are possible. The new structures will be discussed later. On the other hand, the square with $N_s=10$ shows an imaginary frequency along the out-of-plane vibrational mode (B_{2u}) that is not predicted by the FOJT effect. Analysis of the MO's indicates a quasidegeneracy between the HOMO and the LUMO, both of E symmetry, suggesting that a second-order Jahn-Teller SOJT effect could occur. Symmetry analysis of both MO's with respect to the molecular plane indicates that the HOMO is of E_u symmetry while the LUMO is of E_g symmetry. Therefore, only the B_{2u} vibrational mode is involved in the SOJT distortion since it is

TABLE V. Presentation of all the structures of Co_4 optimized at the local level. The $T_d(N_s=12)$, $D_{2h}(N_s=2)$, and $D_{2h}(N_s=0)$ structures have also been optimized and their respective energies are 0.961, 2.091, and 2.535 eV less stable than the $D_{2d}(N_s=10)$ structure.

$N_s=4$		$N_s=6$		$N_s=8$		$N_s=10$	
Structure	Energy[a]	Structure	Energy	Structure	Energy	Structure	Energy
						$D_{2d}^{(1)}$	$\Delta E=0.0$
				D_2	$\Delta E=0.076$		
				D_{2d}	$\Delta E=0.088$		
				D_{2h}^{rhomb}	$\Delta E=0.143$		
						C_{2v}	$\Delta E=0.158$
						D_{2h}^{rhomb}	$\Delta E=0.175$
						D_{2h}^{rect}	$\Delta E=0.260$
						$D_{2d}^{(2)}$	$\Delta E=0.275$
						D_{4h}	$\Delta E=0.295$
				D_{2h}^{rect}	$\Delta E=0.325$		
				D_{4h}	$\Delta E=0.340$		
		T_d	$\Delta E=0.372$				
		D_{2d}	$\Delta E=0.440$				
				T_d	$\Delta E=0.483$		
		D_{2h}^{rect}	$\Delta E=0.796$				
T_d	$\Delta E=0.839$						
		D_{4h}	$\Delta E=0.842$				
						T_d	$\Delta E=0.907$
		D_{2h}^{rhomb}	$\Delta E=0.995$				
D_{4h}	$\Delta E=1.234$						
D_{2h}	$\Delta E=1.847$						

[a] Relative energy compared to the most stable structure $D_{2d}(N_s=10)$ $(E=-5520.115\,379$ a.u.).

the only out-of-plane mode contained in the direct product $(E_u)\times E_g)=A_{1u}+B_{1u}+B_{2u}$.

For T_d structures with $N_s=8$ and 10, the HOMO is triply degenerate with respective occupations of one and two electrons, leading to a T symmetry state susceptible to JT distortion along the E or T_2 vibrational modes, respectively. However, we were not able to calculate the vibrational frequencies due to convergence problems. Nevertheless, both deformations C_{3v} and D_{2d} resulting from the T_2 and E-vibrational modes were investigated. Those deformed structures will be discussed later. The T_d structure with $N_s=6$ shows no partially occupied degenerate MO's. Thus no FOJT distortion occurs. Also, vibrational calculations confirm that this is a real minimum on the potential surface (Table VI).

(b) $D_{2h}^{\text{rhomb}}(N_s=8,10)$ and $D_{2h}^{\text{rect}}(N_s=8,10)$ structures. The LSDA optimized rhombic and rectangular structures with $N_s=8$ and 10, resulting from FOJT distortions, are presented in Fig. 11. Since the two distorsions B_{1g} and B_{2g} of the square are not degenerate (Table VI), there is no reason to expect that they will produce identical energy lowering. In fact, one distorsion is expected to lead to two equivalent minima on the potential surface for the lowest state, while the other should lead to two equivalent transition states connected by minima.[56] In the present case, $D_{2h}^{\text{rhomb}}(N_s=8{,}10)$ structures are more stable than the $D_{2h}^{\text{rect}}(N_s=8{,}10)$ ones at LSDA and GGA levels. At this point, the most stable structure is the $D_{2h}^{\text{rhomb}}(N_s=8)$, which is a real minimum on the potential surface since all its frequencies are real. The $D_{2h}^{\text{rect}}(N_s=8)$ structure, which is 0.257 eV less stable at the GGA level than the $D_{2h}^{\text{rhomb}}(N_s=8)$ one (Table VII), is a transition state along the B_{1g} vibrational mode. Thus the two equivalent $D_{2h}^{\text{rhomb}}(N_s=8)$ structures are connected to each other by two equivalent $D_{2h}^{\text{rect}}(N_s=8)$ structures. The $D_{2h}^{\text{rhomb}}(N_s=10)$, unlike the $D_{2h}^{\text{rhomb}}(N_s=8)$, is not a real minimum on the potential surface since it presents an imaginary frequency for the B_{1u} vibrational mode. Even with a very stringent convergence criterion for the density, the B_{1g} mode of the $D_{2h}^{\text{rect}}(N_s=10)$ structure does not present an imaginary frequency at the GGA level (see Table VI), contrary to what is expected on the basis of the JT theorem. For this case, LSDA frequencies are in better agreement with the JT expectation than are the GGA ones. However, it is necessary to take into account that the lowest frequencies (A_u and B_{1g}) are very low and, considering the accuracy of the frequency calculations (about $50\ \text{cm}^{-1}$), such flat surfaces could yield either real or imaginary frequencies depending on rather small numerical details. To reduce the numerical error introduced in the frequencies, to at least be confident about the sign, it would be necessary to perform those calculations with a more extended grid than the one used here, similar to the situation discussed by Baker *et al.*[37] in another context.

(c) $D_{2d}^{(2)}(N_s=10)$ structure. [This structure with the label (2) comes from a SOJT distortion of the $D_{4h}(N_s=10)$ structure, while the $D_{2d}^{(1)}(N_s=10)$ structures results from a FOJT effect of the $T_d(N_s=10)$ structure.] The optimized geometry and frequencies of the $D_{2d}^{(2)}(N_s=10)$ structure resulting from the SOJT effect of the $D_{4h}(N_s=10)$ structure according to the B_{2u} vibrational mode are presented in Table VI. Since this structure is high in energy compared to the rhombic

TABLE VI. Co_4 LSDA (and GGA in parentheses) bond length and frequencies for the lowest structures.

D_{4h} structure				C_{2v} structure		
		$N_s=8$	$N_s=10$			$N_s=10$
R_e (Å)		2.08	2.09	R_e (Å)		2.09 (2.13)
						2.68 (2.73)
				dihedral angle °		160 (178)
Symmetry	Spectral activity	Frequency (cm^{-1})		Symmetry	Spectral activity	Frequency (cm^{-1})
B_{2g}		$i377$	$i110$	A_1	IR	63 (10)
B_{1g}		$i102$	$i63$	A_1	IR	138 (115)
B_{2u}		62	$i56$	A_2	R	245 (184)
E_u	IR	327	314	B_1	IR,R	289 (263)
E_u	IR	327	314	B_2	IR,R	346 (318)
A_{1g}		356	347	A_1	IR,R	350 (321)

$D_{2h}^{\rm rhomb}$ structure				$D_{2d}^{(2)}$ structure (from square)		
		$N_s=8$	$N_s=10$			$N_s=10$
R_e (Å)		2.13 (2.19)	2.09 (2.13)	R_e (Å)		2.09
		2.27 (2.28)	2.68 (2.73)			2.91
		64 (63)	80 (80)	diedral angle		145
Symmetry	Spectral activity	Frequency (cm^{-1})		Symmetry	Spectral activity	Frequency (cm^{-1})
B_{1u}	IR	3 (58)	$i52$ ($i27$)	B_2	IR	$i82$
A_g		195 (159)	129 (115)	A_1		74
B_{1g}	R	211 (186)	230 (180)	B_1		190
B_{3u}	IR	214 (189)	287 (262)	E	IR,R	312
B_{2u}	IR	350 (317)	350 (321)	E	IR,R	312
A_g		358 (334)	347 (317)	A_1		352

$D_{2h}^{\rm rect}$ structure				
		$N_s=8$	$N_s=10$	
R_e (Å)		2.05 (2.09)	2.05 (2.08)	
		2.11 (2.17)	2.13 (2.19)	
Convergence criteria		$\Delta\rho=10^{-5}$	$\Delta\rho=10^{-5}$	$\Delta\rho=10^{-8}$
Symmetry	Spectral	Frequency (cm^{-1})		
A_u		50 (67)	$i35$ (32)	$i35$ (32)
B_{1g}	R	62 ($i54$)	$i26$ (32)	$i26$ (33)
B_{3u}	IR	308 (269)	295 (260)	295 (260)
A_g		326 (290)	316 (282)	316 (282)
B_{2u}	IR	344 (326)	339 (316)	340 (316)
A_g		369 (349)	359 (339)	359 (339)

D_2 structure			$D_{2d}^{(1)}$ structure (from the tetrahedron)			
		$N_s=8$			$N_s=8$	$N_s=10$
R_e (Å)		2.05 (2.07)	R_e (Å)		2.09 (2.14)	2.09 (2.13)
		2.15 (2.22)			2.49 (2.58)	2.65 (2.77)
		2.49 (2.59)	dihedral angle		115 (105)	127 (129)
Symmetry	Spectral activity	Frequency (cm^{-1})	Symmetry	Spectral activity	Frequency (cm^{-1})	
B_3	IR,R	76 (53)	B_1		$i85$ ($i103$)	277 (259)
A		145 (133)	B_2	IR	66 ($i33$)	128 (108)
A		190 (195)	A_1		150 (138)	104 (94)

TABLE VI. (*Continued*).

Symmetry	Spectral activity	Frequency (cm^{-1})	Symmetry	Spectral activity	Frequency (cm^{-1})	
B_2	IR,R	262 (232)	E	IR,R	306 (278)	303 (285)
B_1	IR,R	348 (343)	E	IR,R	306 (279)	303 (285)
A		401 (387)	A_1		397 (366)	381 (351)

T_d structure

		N_s=6
R_e (Å)		2.18
Symmetry	Spectral activity	Frequency cm^{-1}
E		172
E		172
T_2	IR	256
T_2	IR	256
T_2	IR	256
A_1		356

ones, only LSDA calculations were performed. This structure, 0.02 eV more stable than the $D_{4h}(N_s=10)$ one, is susceptible to distorsion according to the B_2 and B_1 JT active modes since it has a degenerate half-occupied HOMO. Vibrational calculations show that only the B_2 mode is JT active.

(d) $C_{3v}(N_s=8,10)$ and $D_{2d}^{(1)}(N_s=8,10)$ structures. Both $C_{3v}(N_s=8,10)$ and $D_{2d}^{(1)}(N_s=8,10)$ structures resulting from

TABLE VII. Comparison of the relative stability of some of the low-lying structures of the tetramer of cobalt computed at different levels of geometry optimization and SCF approximation (geometry optimization level)/(SCF level).

Structure				Geometry in Å and degree		Relative stability (eV)		
Symmetry	N_s	Dimension	Nature	Local	Nonlocal	LSDA/LSDA[a]	LSDA/GGA[b]	GGA/GGA[c]
$D_{2d}^{(1)}$	10	3D	RM[d]	2.09	2.13	0.000	0.069	0.000
				2.65	2.77			
C_{2v}^{rhomb}	10	3D	RM	2.09	2.13			
				2.68	2.73	0.158	0.126	0.093
				160	178			
D_{2h}^{rhomb}	10	2D	TS[e]	2.09	2.13	0.175	0.000	0.094
				2.68	2.73			
D_{2h}^{rhomb}	8	2D	RM	2.13	2.19	0.143	0.110	0.140
				2.27	2.28			
D_{2h}^{rect}	10	2D	RM	2.05	2.08	0.260	0.233	0.195
				2.13	2.19			
D_{2d}	8	3D	JT[f]	2.09	2.14	0.088	0.222	0.316
				2.49	2.58			
D_2	8	3D	RM	2.05	2.07	0.076	0.356	0.324
				2.15	2.22			
				2.49	2.59			
D_{2h}^{rect}	8	2D	TS	2.05	2.09	0.325	0.429	0.397
				2.11	2.17			

[a] LSDA/LSDA energy reference: $D_{2d}^{(1)}(N_s=10)$, $E=-5520.115\,379$ a.u.

[b] LSDA/GGA energy reference: $D_{2h}^{\text{rhomb}}(N_s=10)$, $E=-5531.500\,296$ a.u.

[c] GGA/GGA energy reference: $D_{2d}^{(1)}(N_s=10)$, $E=-5531.503\,719$ a.u.

[d] Real minimum on the potential surface (refer to Table VI at the GGA level).

[e] Transition state on the potential surface (refer to Table VI at the GGA level).

[f] JT point on the potential surface (refer to Table VI at the GGA level).

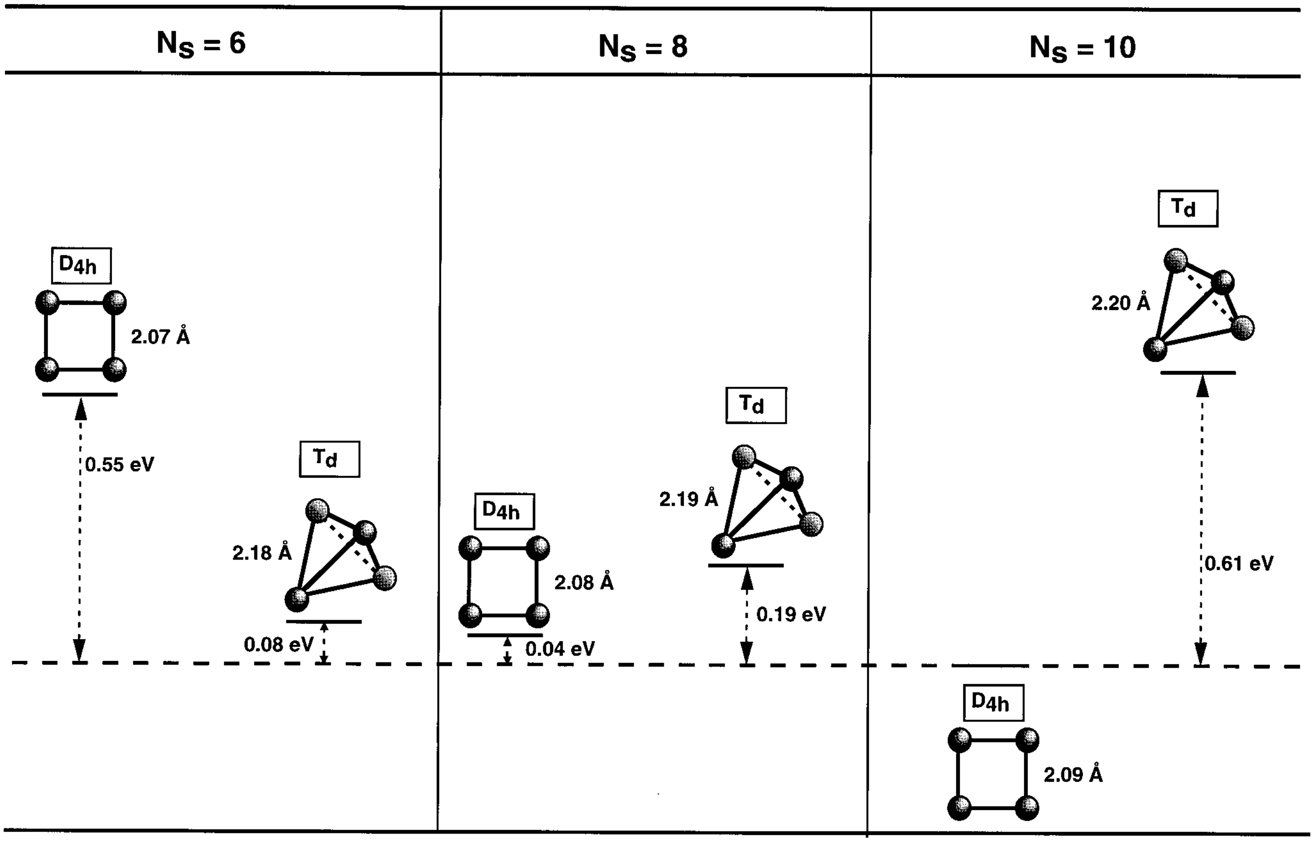

FIG. 10. Relative stability of the Co_4 highly symmetric LSDA optimized structures.

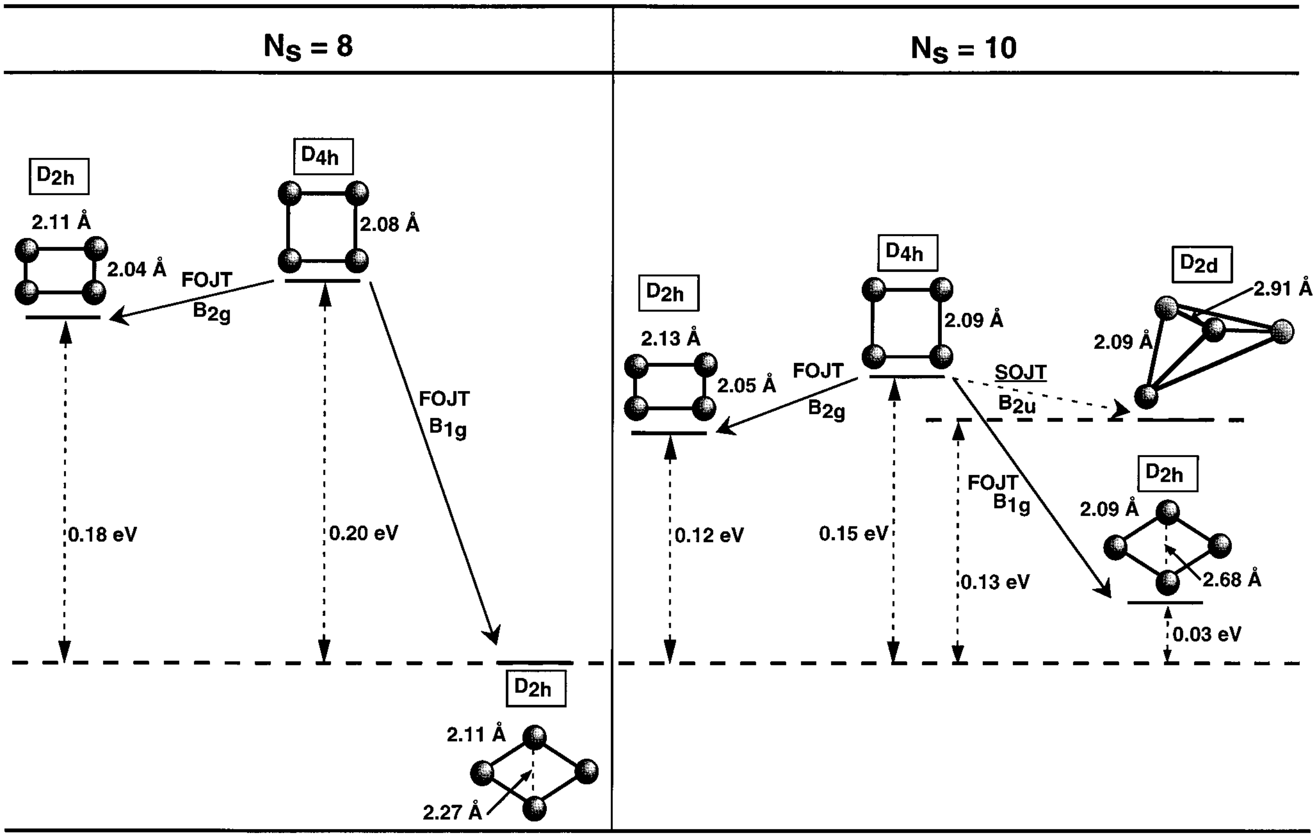

FIG. 11. Relative stability of Co_4 planar distorted structures.

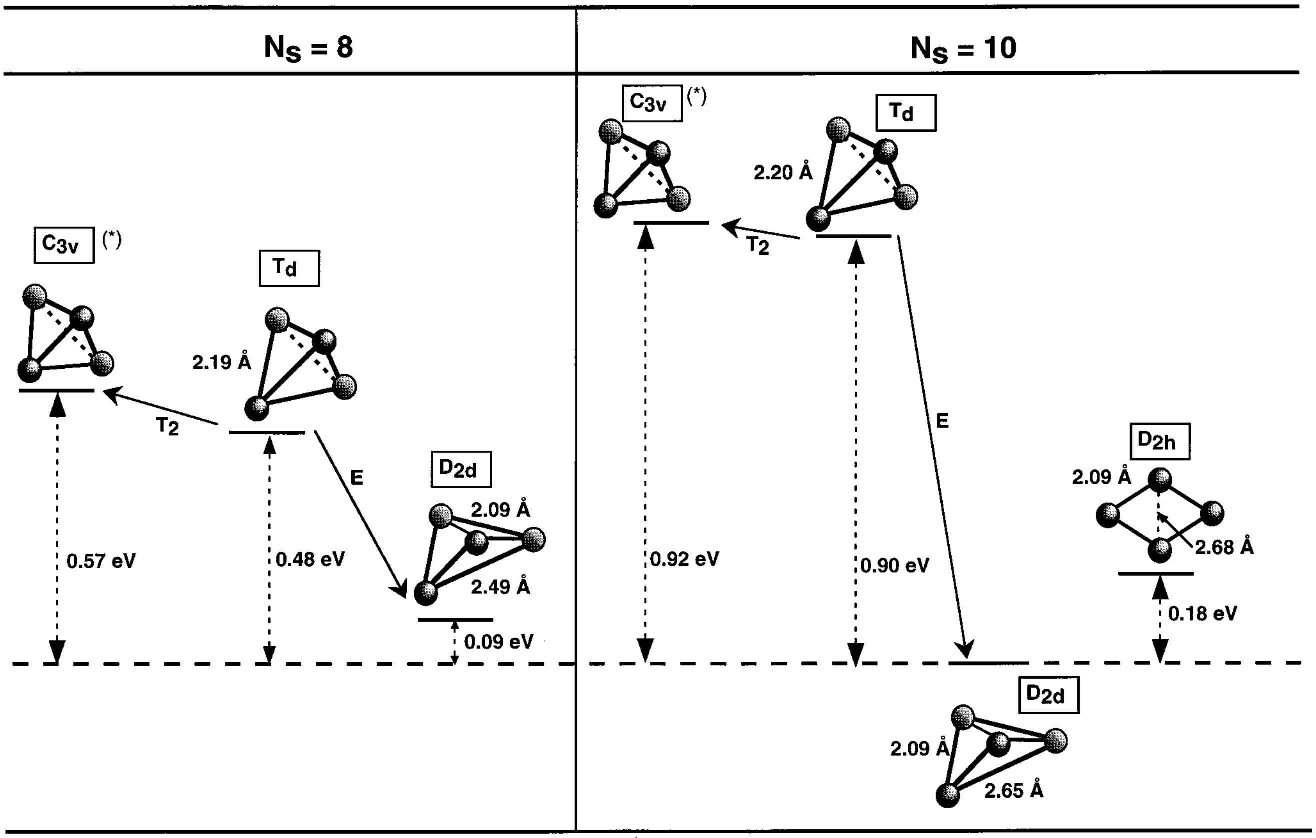

FIG. 12. Relative stability of 3D Co_4 distorted structures.

the deformation of the $T_d(N_s=8,10)$ structures according to the JT active mode T_2 and E are presented at the LSDA level in Fig. 12. The $C_{3v}(N_s=8,10)$ structures presented here correspond in fact to a single-point calculation where one of the $T_d(N_s=8,10)$ bond lengths was increased by 0.1 Å. Those structures are less stable than the T_d ones. On the other hand, the $D_{2d}^{(1)}(N_s=8,10)$ optimized structures lead to an important stabilization. Among all the structures optimized, the $D_{2d}^{(1)}(N_s=10)$ structure is the most stable one. This structure has all of its frequencies real (Table VI) and its MO's have integer occupation numbers. Therefore, at this point, it appears to be the ground state of the Co_4 cluster. The $D_{2d}^{(1)}(N_s=8)$ structure, whose HOMO is doubly degenerate and half occupied, has two imaginary frequencies (in the GGA calculations) active by the FOJT theorem. The B_1 and B_2 vibrational modes lead to a D_2 and C_{2v} symmetrical structures, respectively, which will be discussed in the following paragraph.

(e) $D_2(N_s=8)$ and *$C_{2v}(N_s=8)$ structures.* The optimized LSDA and GGA $D_2(N_s=8)$ structures are minima on the potential surface (Table VI). At the LSDA level, the $D_2(N_s=8)$ structure is 0.01 eV more stable than the $D_{2d}^{(1)}(N_s=8)$ one, while at the GGA level, we observed a destabilization of 0.01 eV. Results obtained at the GGA level are in disagreement with the behavior of the $D_{2d}^{(1)}(N_s=8)$ frequencies showing an imaginary frequency of $103i$ cm^{-1} for the B_1 mode. For this structure, it should be necessary to perform the calculation with an extended grid. Despite the computed GGA imaginary frequency of B_2 symmetry (see Table VI), geometry optimization of the $C_{2v}(N_s=8)$ structure obtained from this deformation always gives back the $D_{2d}(N_s=8)$ structure. Single-point calculations were also performed at both the LSDA and GGA levels. An augmentation of the energy with the deformation was observed and thus we conclude that the GGA imaginary frequency is an artifact.

(f) $D_{2h}^{\mathrm{rhomb}}(N_s=10)$ transition state. The $D_{2h}^{\mathrm{rhomb}}(N_s=10)$ structure is a transition state on the potential and has an imaginary frequency according to the B_{1u} vibrational mode (out-of-plane) leading to a $C_{2v}(N_s=10)$; structure, see Table VI. An optimization of geometry according to this mode leads to a dihedral angle very different for the LSDA and GGA levels. This structure is a real minimum on the potential surface.

(g) Ground state $D_{2d}^{(1)}(N_s=10)$ and its spectroscopic constants. Table VIII presents the properties for the most stable structure calculated in this work. The absolute minimum corresponds to the $D_{2d}^{(1)}(N_s=10)$ structure. The bond length increases in going from the LSDA to the GGA level, while the

TABLE VIII. Comparison of properties calculated at LSDA and GGA levels for the ground state of Co_4, $D_{2d}(N_s=10)$.

			D_e (eV)	
	R_e (Å)	Frequencies (cm^{-1})	IP (eV)	Vertical
LSDA	$r_1=2.09$	104,128,277		6.89
	$r_2=2.65$	303,303,381		
GGA	$r_1=2.13$	94,108,259	7.89	7.02
	$r_2=2.77$	285,285,351		

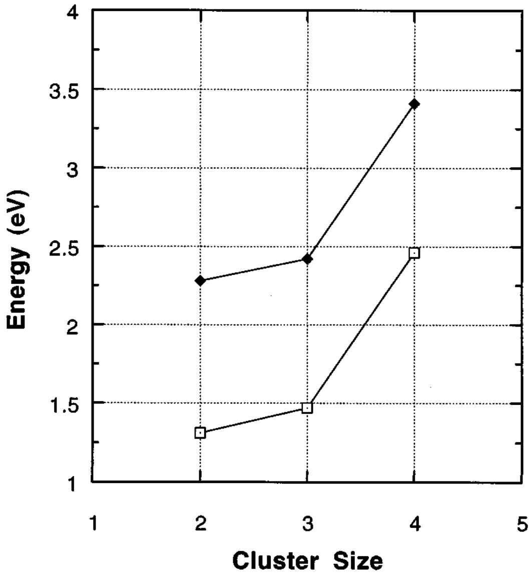

FIG. 13. Attachment energy in eV. The square corresponds to experimental results and the dots are our results.

dihedral angle remains the same. The binding energy has been calculated only at the GGA level.

2. Assessment of the accuracy of results

A summary of the most stable structures is presented in Table VII. The optimized geometry at LSDA and GGA levels are included as well as the relative stability compared to the most stable structure. The fifth column presents LSDA results and the seventh GGA results. The sixth column entitled LSDA/GGA presents SCF calculations performed at the GGA level with the geometry optimized at the LSDA level. The most stable structure is the $D_{2d}^{(1)}(N_s=10)$ structure at both levels. In general, the structures are almost degenerate and their relative stability varies according to the type of calculation. This table points out that for transition metals the LSDA/GGA type of calculation are not reliable because the geometry obtained between LSDA and GGA are different and because the relative stability differs from LSDA/GGA to GGA/GGA. Thus, for this kind of compound, a GGA/GGA calculation is necessary in order to get the most precise results. Also, it should be interesting to know the influence of an extended grid for this kind of cluster.

V. GENERAL TRENDS

The number and size of clusters considered herein is sufficiently large to try to establish some general trends. First, we define the attachment energy $E_a(n)$ of a cluster of size n as

$$E_a(n)=E(\mathrm{Co}_n)-[E(\mathrm{Co}_{n-1})+E(\mathrm{Co})]. \qquad (5.1)$$

We have computed the attachment energy at the GGA level using the NS approximation as the reference atomic energy. Results are presented in Fig. 13 along with the experimental values taken from Ref. 2 Despite an average difference of 0.9 eV, we can see that the theoretical trend is in agreement with the experimental results. The absolute value of the attachment energy, which depends strongly on the quality of the computed energy of the atom, should improve with the ability of the functional to correctly describe atomic behavior.

TABLE IX. First-order JT active modes for several molecular symmetries.

Molecular symmetry	Electronic symmetry	JT active mode	Reduced symmetry
D_{3h}	E'	E'	C_{2v}
T_d	T_1 or T_2	E	D_{2d}
		T_2	C_{3v}
D_{4h}	E_g	B_{1g}	D_{2h}^{rhomb}
		B_{2g}	D_{2h}^{rect}
D_{2d}	E	B_1	D_2
	B_2	C_{2v}	

Magnetic properties of cobalt clusters have been studied experimentally[7,9] as well as theoretically.[57] It has been proposed by Khanna and Linderoth[8] that cobalt clusters have a superparamagnetic behavior. The average magnetic moment per atom was computed for the most stable structures for each cluster. We find values larger than that of bulk Co $(1.727\mu_B)$ for the moment per atom μ, namely, $\mu=2\mu_B$ for Co_2, $1.67\mu_B$ and $2.33\mu_B$ for Co_3, and finally $2\mu_B$ and $2.5\mu_B$ for the tetramer.

VI. CONCLUSION

With the technical parameters chosen (basis sets, grids, etc.) we believe the results represent the limit, for a given functional, to within about 0.05 Å for bond lengths, 50 cm^{-1} for frequencies, and a few tenths of an eV for relative energies. Higher precision would require, in particular, a more extensive radial grid.

The dimer ground state was found to be of $\Delta_g(N_s=4)$ symmetry state with a bond length of 2.01 Å and a frequency of 342 cm^{-1}. At the LSDA level, the most stable trimer was found to be the obtuse triangle with $N_s=5$. We have shown that this structure is practically degenerate with the acute triangle of the same spin state, while the obtuse triangle with $N_s=7$ is 0.22 eV higher. At the GGA level, this difference was reduced to nearly zero (0.07 eV). Those small energy differences oblige one to think about those systems not in terms of rigid structures but rather in terms of dynamical averages over nuclear positions. The situation is more complicated for Co_4, where we found five GGA structures, which are real minima, in the range of 0.4 eV. Three of them are three-dimensional structures, the others being planar. Three of them have $N_s=10$, while the others have $N_s=8$. The most stable structure computed is the $D_{2d}^{(1)}(N_s=10)$ structure obtained from a IT deformation of the tetrahedron (Table IX). Finally, the computed attachment energies follow the same trend as the experimental values and the magnetic moment seems to increase with the cluster size if only the highest spin state is considered.

ACKNOWLEDGMENTS

C.J. thanks Normand Desmarais for his helpful discussions and Mark Casida for comments on this manuscript. A.M. thanks the Laboratorio de Visualizacion y Computo en Paralelo (UAM-iztapalapa, Mexico) for computing time. Financial support from NSERC Canada and FCAR Québec is gratefully acknowledged as are computing resources of the Services Informatiques de l'Université de Montréal.

---

[1] A. Kant and B. Strauss, J. Chem. Phys. **41**, 3806 (1964).

[2] D. A. Hales, C.-X. Su, L. Lian, and P. B. Armentrout, J. Chem. Phys. **100**, 1049 (1994).

[3] D. P. Di Lella, W. Limm, R. H. Lipson, M. Moskovits, and K. V. Taylor, J. Chem. Phys. **77**, 5263 (1982).

[4] J. G. Dong, Z. Hu, R. Craig, J. R. Lombardi, and D. M. Lindsay, J. Chem. Phys. **101**, 9280 (1994).

[5] D. G. Leopold and W. C. Lineberger, J. Chem. Phys. **85**, 51 (1986).

[6] E. K. Parks, T. D. Klots, and S. J. Riley, J. Chem. Phys. **92**, 3813 (1990).

[7] D. C. Douglas, A. J. Cox, J. P. Bucher, and L. A. Bloomfield, Phys. Rev. B **47**, 12 874 (1993).

[8] S. N. Khanna and S. Linderoth, Phys. Rev. Lett. **67**, 742 (1991).

[9] J. P. Bucher, D. C. Douglas, and L. A. Bloomfield Phys. Rev. Lett. **66**, 3052 (1991).

[10] H. P. Cheng, R. S. Berry, and R. L. Whetten, Phys. Rev. B **43**, 10 647 (1991).

[11] V. Bonacic-Koutecky, L. Cespiva, P. Fantucci, and J. Koutecky, J. Chem. Phys. **98**, 7981 (1993).

[12] D. M. Cox, D. J. Trevor, R. L. Whetten, and A. Kaldor, J. Phys. Chem. **92**, 421 (1988).

[13] J. M. Broto, J. C. Ousset, H. Rakoto, S. Askenazy, Ch. Dufor, M. Brieu, and P. Mauret, Solid State Commun. **85**, 263 (1993).

[14] A. J. Cox, J. G. Louderback, and L. A. Bloomfield, Phys. Rev. Lett. **71**, 923 (1991).

[15] R. A. Groglia, J. M. Pacheco, and C. Yannouleas, Phys. Rev. B **44**, 5901 (1991).

[16] *Metal Clusters*, edited by M. Moskovits (Wiley, New York, 1986).

[17] W. F. Cooper, G. A. Clarke, and C. R. Hare, J. Chem. Phys. **78**, 2268 (1972).

[18] A. Wolf and H.-H. Schmidtke, Int. J. Quantum Chem. **18**, 1187 (1980).

[19] I. Shim and K. A. Gingerich, J. Chem. Phys. **78**, 5693 (1983).

[20] J. Harris and R. O. Jones, J. Chem. Phys. **70**, 830 (1979).

[21] L. Goodwin and D. R. Salahub, Phys. Rev. A **47**, 774 (1993).

[22] M. Castro and D. R. Salahub, Phys. Rev. B **49**, 11 842 (1994).

[23] D. S. Yang, M. Z. Zgierski, D. M. Rayner, P. A. Hackett, A. Martinez, D. R. Salahub, P. N. Roy, and T. Carrington, Jr., J. Chem. Phys. **103**, 5335 (1995).

[24] A. St-Amant and D. R. Salahub, Chem. Phys. Lett. **169**, 387 (1990).

[25] D. R. Salahub, R. Fournier, P. Mlynarski, I. Papai, A. St-Amant, and J. Ushio, in *Density Functional Methods in Chemistry*, edited by J. Labanowski and J. Andzelm (Springer, Berlin, 1991).

[26] S. H. Vosko, L. Wilk, and M. Nusair, Can. J. Phys. **58**, 1200 (1980).

[27] J. P. Perdew and Y. Wang, Phys. Rev. B **33**, 8800 (1986).

[28] J. P. Perdew, Phys. Rev. B **33**, 8822 (1986).

[29] J. P. Perdew, Phys. Rev. B **34**, 7406(E) (1986).

[30] DEMON. User's guide, version 1.0 beta, Biosym Technologies, San Diego, 1992.

[31] N. Godbout (private communication). In the spirit of N. Godbout, D. R. Salahub, J. Andzelm, and E. Wimmer, Can. J. Chem. **70**, 560 (1992).

[32] See H. B. Schlegel, in *Ab Initio Methods in Quantum Chemistry–I*, edited by K. P. Lawlwy (Wiley, New York, 1987).

[33] R. Carbo, J. A. Hernandez, and F. Sanz, Chem. Phys. Lett. **47**, 581 (1977).

[34] E. Radzio, J. Andzelm, and D. R. Salahub, J. Comput. Chem. **6**, 533 (1985).

[35] A. Goursot, I. Papai, and C. A. Daul, Int. J. Quantum Chem. **52**, 799 (1994).

[36] S. Chrétien and D. R. Salahub (unpublished).

[37] J. Baker, J. Andzelm, A. Scheiner, and B. Delley, J. Chem. Phys. **101**, 8894 (1994).

[38] O. Gunnarsson and B. I. Lundquist, Phys. Rev. B **13**, 4274 (1976).

[39] U. von Barth, Phys. Rev. A **20**, 1693 (1979).

[40] J. Harris and R. O. Jones, J. Chem. Phys. **68**, 3316 (1978).

[41] O. Gunnarsson and R. O. Jones, J. Chem. Phys. **72**, 5357 (1980).

[42] F. W. Kutzler and G. S. Painter, Phys. Rev. Lett. **12**, 1285 (1987).

[43] R. P. Messmer and D. R. Salahub, J. Chem. Phys. **65**, 779 (1976).

[44] T. Ziegler, A. Rauk, and E. J. Baerends, Theor. Chim. Acta **43**, 261 (1977).

[45] C. Daul, Int. J. Quantum Chem. **52**, 867 (1994).

[46] C. Jamorski, M. E. Casida, and D. R. Salahub, J. Chem. Phys. **104**, 5134 (1996).

[47] C. E. Moore, *Atomic Energy Levels*, Natl. Bur. Stand. (U.S.) Circ. No. 467 (U.S. GPO, Washington, 1971).

[48] P. Mlynarski and D. R. Salahub, Phys. Rev. B **43**, 1399 (1991).

[49] B. Simard (private communication).

[50] L. M. Russon, S. A. Heidecke, M. K. Birke, J. Conceicao, M. D. Morse, and P. B. Armentrout, J. Chem. Phys. **100**, 4747 (1994).

[51] P. A. Montano and G. K. Shenoy, Solid State Commun. **35**, 53 (1980).

[52] H. Purdum, P. A. Montano, G. K. Shenoy, and T. Morisson, Phys. Rev. B **25**, 4412 (1982).

[53] M. D. Morse *et al.*, Phys. Rev. B **30**, 5400 (1984).

[54] M. Tomonari and H. Tatewaki, J. Chem. Phys. **88**, 1828 (1988).

[55] I. B. Bersuker, *The Jahn-Teller Effect and Vibronic Interactions in Modern Chemistry* (Plenum, New York, 1984).

[56] G. Herzberg, *Molecular Spectra and Molecular Structure* (Van Nostrand, New York, 1966), Vol. 3, p. 44.

[57] Z. Q. Li and B. L. Gu, Phys. Rev. B **47**, 13 611 (1993).